Int J Adv Manuf Technol (2016) 87:1985–1997
DOI 10.1007/s00170-016-8587-3

ORIGINAL ARTICLE

Development of a new combined heat source model for welding based on a polynomial curve fit of the experimental fusion line

Junqiang Wang[1] · **Jianmin Han**[1] · **Joseph P. Domblesky**[2] · **Zhiyong Yang**[1] · **Yingxin Zhao**[1] · **Qiang Zhang**[1]

Received: 3 November 2015 / Accepted: 2 March 2016 / Published online: 15 March 2016

Abstract To improve the accuracy of finite element (FE) models used to simulate electric arc and beam-based fusion welding processes, a combined heat source model is proposed. The combined model, termed the polynomial heat source, is based on a Gaussian heat density distribution and employs a disc source to account for surface heating effects while a polynomial equation is used to define the volumetric heat power source. This provides an improved capability for matching the heat source power distribution to fusion zones having variable curvature and also results in a simplified process for defining heat source parameters as only three numerical values need to be determined. To validate the heat source model, fusion zone cross sections, thermal cycles, angular distortion, and residual stresses obtained using SYSWELD were compared to measurements taken from gas metal arc (GMA) welds made on 10-mm-thick high-strength low-alloy (HSLA) plates. Predictions obtained from SYSWELD using double ellipsoid and conical heat source models were also compared. An analysis of the FE predictions obtained from each of the three heat source models showed that the best agreement between simulated and experimental values was achieved using the polynomial model. This is attributed to the fact that heat power distribution can be adjusted at the top and bottom of the fusion zone and results in an improved level of bead cross section matching. It is expected that the proposed heat source model will be applicable for simulating both shallow and deep penetration welding processes where the fusion zone is symmetric about its centerline.

Keywords Gaussian heat source · Finite element modeling · Welding distortion · Residual stress · GMA welding

✉ Jianmin Han
jmhan@bjtu.edu.cn

[1] School of Mechanical, Electronic and Control Engineering, Beijing Jiaotong University, Beijing 100044, People's Republic of China

[2] Mechanical Engineering Department, Marquette University, 1515 West Wisconsin Avenue, Milwaukee, WI 53201-1881, USA

1 Introduction

Fully coupled finite element (FE) models that can simulate moving heat sources and predict the resulting temperature fields and mechanical properties of a weldment have become widely used in industry. However, it is well established that the simulation accuracy of an FE process model is heavily dependent on the heat source model that is used [1]. Not only does the heat source model define the thermal history used to simulate welding, it also has a direct impact on the accuracy of numerical predictions related to weld strength, distortion, residual stresses, and phase changes. As it is difficult to directly validate a heat source model on the basis of measurements of power density and temperatures in the weld pool, accuracy is typically assessed on the basis of how well the geometry of the simulated and actual weld bead cross sections match. Consequently, it must be considered that a heat source model tends to provide reduced accuracy when the actual weld bead cross section deviates from the geometry assumed in the source model. For example, the use of a double ellipsoid heat source model necessitates that the fusion zone cross section closely approximates an elliptical shape whereas a trapezoidal cross section would be required for a conical heat source. Although many welds can be reasonably represented using such shapes, fusion zones that possess irregular or varying curvature such as nailhead geometries are more problematic. While such welds can be modeled using combined heat

sources, e.g., compound double ellipsoid, this can result in increased simulation effort and modeling complexity and suggests that a simplified model having comparable flexibility would be useful.

A second consideration is that simulation accuracy is also highly dependent on the values of the parameters that are used in a heat source model. As thermal transfer from an actual heat source to a weld represents a complex set of phenomenon, the parameters for most heat source models cannot be directly determined from the welding conditions used. Instead, they must be calculated for an individual welding process based on estimated weld pool dimensions or inverted from an actual weld bead cross section using an optimization algorithm or trial and error. From a practical perspective, the effort required to obtain these values tends to be proportional to the number of coefficients used in the heat source model. As a result, a heat source model that minimizes the number of parameters used and/or reduces the engineering effort needed to describe the thermal power distribution will also be beneficial.

The Gaussian heat source, often referred to as a disc source, was first proposed by Pavelic et al. [2]. This provided improved temperature predictions over those obtained using Rosenthal's point source model [3] and differed from previous analyses in that heat input to the workpiece was considered to be distributed over a defined surface area. Subsequent work has mainly focused on distributed sources though a modified point source model was proposed by Wenji et al. [4], who incorporated the effect of temperature-dependent material properties as the basis for a real-time process control scheme. While the disc heat source provided improved accuracy, several researchers such as Goldak et al. [5] have noted that it does not reflect the digging and stirring action of the arc which causes significant heating effects within the weld pool and must be considered when modeling deep penetration welds. Consequently, the use of the disc heat source is often limited to modeling shallow penetration welds having a large width.

To better incorporate heating effects within the weld pool, Paley and Hibbert [6] proposed replacing the disc source with a volume heat source having a uniform heat power density. A later volumetric heat source termed the double ellipsoid model was proposed by Goldak et al. [5]. The double ellipsoid heat source model differed in that a Gaussian heat density distribution was used and enabled asymmetric fusion zone geometries having elliptical cross sections to be represented. However, the double ellipsoid model does have somewhat limited capability for simulating narrow, nonconvex fusion zones which frequently develop in the case of laser and electron beam welding as well as irregular, highly curved fusion zones exemplified by the "nailhead" weld bead. An alternative volume heat source model proposed by Wu et al. [7] was based on a Gaussian curve which was inverted and rotated around the centerline in order to generate the fusion zone geometry. By adjusting the parameters, the rotary Gaussian volume heat source model is able to represent a nailhead-shaped fusion zone and, as such, is well suited for simulating high-energy beam welding processes. Li et al. [8] employed this heat source to simulate laser welding of dual phase steel and were able to achieve good agreement with experimental results. However, the rotary Gaussian model requires that the weld bead has a bell-shaped cross section and, as a result, is not well suited for trapezoidal cross sections which can be better represented using a cylindrical or conical heat source model.

In an effort to achieve improved agreement between predicted and actual fusion zone geometries in specific fusion welding processes, combined heat source models as well as compound volume sources have been used. A combined heat source using both surface and volume heat source components was proposed by Bachorski et al. [9] for arc welding. In this model, a disc source is used to simulate radiation heating from the arc, while weld pool heating, considered to be due to the heat content of metal droplets from a consumable electrode, is modeled using a cylindrical volume source component. Chen et al. [10] proposed a combined heat source model for arc welding which also employed a disc source to represent radiation heating effects but employed a double ellipsoid source to simulate heating in the weld pool. This resulted in a heat source model with somewhat improved capability for simulating fusion zone boundaries having irregular curvature but required a larger number of input parameters to be determined. Other heat source models have been specifically developed for simulating high-energy beam and hybrid welding processes using compound volume source models. Faraji et al. [11] proposed using trapezoidal and cylindrical heat source models to simulate heat and mass transfer in a hybrid laser–tungsten inert gas welding process. Meng et al. [12] also developed a compound heat source model to simulate laser–metal inert gas welding of an Al alloy and galvanized steel in an effort to address simulation problems associated with dissimilar metals. In this model, the laser beam was modeled as a simple disc source while the electric arc was represented using a 2D double ellipse heat source in conjunction with a uniform volume distribution to account for evaporation of the zinc coating and heat content of the molten metal droplets, respectively. In an effort to evaluate which heat sources provided the most accurate simulation results for pulsed laser welding, the performance of conical, double ellipsoid, and cylindrical heat source models were compared in a study by Chukkan et al. [13]. Combined models based on double ellipsoid-conical and cylindrical-conical heat sources were also considered. Their results showed that having the capability to adjust power at the top and bottom of the fusion zone in a heat source model enabled a closer match between the predicted and actual fusion zone and that this tended to improve the accuracy of the numerical predictions.

In the current study, a combined heat source model composed of surface and volume thermal source components is

presented. The basis for using a disc surface source in conjunction with a polynomial function to represent the volume component is discussed. A description of the simplified inversion technique and polynomial curve fitting process for the volume heat source is also presented along with example fits for representative fusion welds. Simulation results from the proposed polynomial heat source model are assessed by comparing the predicted fusion zone cross section, thermal cycles, residual stress, and angular distortion obtained from SYSWELD against experimental results obtained from butt-welded plates. Corresponding results obtained from FE simulations based on double ellipsoid and conical heat source models are also compared and discussed.

2 Development of the combined heat source model

Computational modeling of fusion welding is divided into two main areas. The first area deals with using comprehensive unified models of the anode, cathode, and plasma to study transport phenomenon. The second area is mainly directed toward understanding and predicting properties of the weld. Consequently, these models tend to focus on simulating phenomena in the workpiece, some of which include the molten weld pool, rather than in the arc plasma or beam source. To reduce computational complexity, the heat source is in most cases incorporated through a boundary condition applied on the surface of the workpiece and/or weld pool. As a result, most heat source models used to simulate industrial joining process are based on a simplified conduction-based model which in principle incorporates both heating at the surface and stirring/digging effects in the weld pool in a single volumetric source. While this represents a suitable solution for some welds, one consequence of using a single function is that it effectively couples surface and volumetric heating. This in effect fixes or defines the boundary condition representing thermal transfer to the workpiece. While this is beneficial in that it facilitates determination of a heat flux value to be used, Murphy et al. [14] have noted that for arc welding, using fixed boundary conditions results in strong limitations and that models using such conditions cannot be depended on to reliably predict weld pool geometry and depth for a wide variety of common welding situations. This further indicates that a more flexible heat source would be useful in improving the ability to match predicted and actual fusion zone geometries.

While a variety of mathematical functions have been proposed for use in heat source models, there is some evidence to suggest that the form of the equation used to represent the volume source may not be as critical as it is to achieve a suitable level of cross section matching between the actual and predicted fusion zones. For example, Chukkan et al. [13] noted that if a high level of bead cross section matching was achieved, the use of different heat source models appeared to have little discernible effect on predicted thermal cycles in laser welding. Additional support comes from Carmignani et al. [15] who simulated laser welding of steel plates using a uniform volumetric power distribution applied over a rectangular section as opposed to using a cylindrical section having a Gaussian distribution. Carmignani et al. [15] noted that the calculated transient thermal field appeared to be rather insensitive to details in the shape of the volumetric source distribution used in the simulation model. This further supports the idea that different mathematical functions can be employed in developing a heat source model.

While many weld beads can be represented using simple geometric shapes such as a hemisphere or ellipse, fusion zones have varying curvature represent special challenges for a heat source model. As noted earlier, the most notable example of this is the "nailhead" weld bead [16, 17]. Upon examination, the nailhead weld bead can be seen to consist of a wide, shallow fusion zone near the surface that is connected to a narrow, deeper penetration zone. As such, it is considered that the geometry of the top section (i.e., the head of the nail) can be well represented using a simple disc heat source in conjunction with a volume heat source to represent the remainder of the fusion zone. Because of its flexibility and simplicity, a polynomial function represents a useful candidate for defining the volume heat source term. An additional advantage is that a suitable polynomial function can be developed directly from the actual weld cross section as described below.

2.1 Polynomial curve fitting procedure

A polynomial fit of the fusion zone can easily be performed using a Cartesian coordinate system if the crown is neglected and the fusion zone is assumed to be symmetric about its centerline such that only half of the weld bead needs to be considered. As an example, consider a butt-welded plate where the long transverse or width direction is defined as the x-axis, the welding direction is taken to be along the y-axis, and the short transverse or thickness direction is defined as the z-axis. Assigning point O as the origin, the coordinate system can be located on the centerline and the x-axis taken to be coincident with the upper surface of the plate for convenience. Consequently, a polynomial function having the general form shown in Eq. (1) can be used to represent the fusion zone cross section.

$$x = a + bz + cz^2 + dz^3 + ez^4 \tag{1}$$

where x represents the half width of the weld bead at some distance z from the top surface of the plate, and a, b, c, d, and e are the coefficients of the polynomial function.

The general procedure for fitting an nth order polynomial to the fusion zone can be described as follows. After exposing

a transverse section of the weld, the fusion line can be photographed and digitized. A suitable grid can then be superimposed on a digital image of the weld cross section as shown in Fig. 1 such that any points on the fusion zone boundary which are coincident with the grid lines are used as data points for curve fitting. Because the goodness of the polynomial curve fit is affected by the accuracy of the data points used, a suitable grid size and sufficient number of data points are needed. While data collection can be done manually, this effort is greatly facilitated by the use of imaging tools such as Visio and AutoCAD which provide enhanced resolution and enable the coordinates of each data point to be obtained with a suitable level of precision. A statistical or data analysis software program can then be used to fit a least square curve polynomial curve of suitable order to the data points and to calculate the coefficients.

To demonstrate the procedure, data points were obtained for the weld shown in Fig. 1 using a 1-mm × 1-mm grid and these are summarized in Table 1. Based on a least squares fit of the data, a fourth order polynomial was found to provide a suitable fit to the fusion line and the resulting polynomial equation was found to be

$$x = 8.8263494 + 2.774984639z + 0.55631947z^2 + 0.034893z^3 + 0.0007104458z^4 \quad (2)$$

where the value of x, z, and the leading coefficient on the right-hand side are given in millimeters. The second coefficient is dimensionless, while the remaining three have units of per millimeter, per square millimeter, and per cubic millimeter, respectively.

Figure 2 shows a comparison of the polynomial curve fit and actual fusion zone geometry obtained from the GMA weld cross section. The correlation coefficient r was found to be 0.994 which indicates a high level of agreement between Eq. (2) and the actual fusion zone cross section. The difference in area between the predicted and actual cross sections was also calculated using digitized images and was found to be less than 3 % which further confirms the goodness of fit.

To illustrate the utility of using a polynomial equation, curve fits were applied to representative weld cross sections having different curvature. The first case is a wide, shallow penetration weld, e.g., bead-on-plate, where the fusion zone can be represented as a fourth order polynomial as shown in Fig. 3a. For the second case where a single pass, full penetration butt weld is considered, a second order polynomial is easily fitted as shown in Fig. 3b. For a deep, narrow weld which is typically made by laser or high-energy plasma welding, a fourth order polynomial curve can also be used as shown in Fig. 3c. These examples demonstrate that a variety of fusion zone geometries can be represented by a suitable order polynomial equation, and it is expected that most weld beads can be represented using a curve of four orders or less.

2.2 Development of the polynomial heat source model

Although the interaction between a heat source and weldment represents a complex set of phenomenon, it is well established that the surface and volumetric heat flux distribution for electric arc, beam, and flame sources can be represented using a Gaussian function which is depicted in Fig. 4. In the case of high-energy beam sources, additional heating is often supplied by a cloud of vaporized metal that forms directly above the weld pool and would also suggest the need for an additional heat source to supplement the volume component. A discussion regarding the use of a combined heat source for beam processes can be found in Luo et al. [18].

With respect to incorporating a disc source in conjunction with a volumetric source for arc welding, the physical basis for this can be understood as follows. It is well known from arc physics that the anode and cathode sheaths act to govern current density, thermal efficiency, and heat flux on the surface of the anode and cathode [19]. However, while these sheaths or layers are necessary to account for coupling between the arc and weld pool in a model, they in a sense represent discontinuities as they tend to be on the order of 2 μm and do not fulfill the conditions for local thermodynamic equilibrium (LTE). Although these layers have been simulated in comprehensive, unified FE models of GMA welding, other

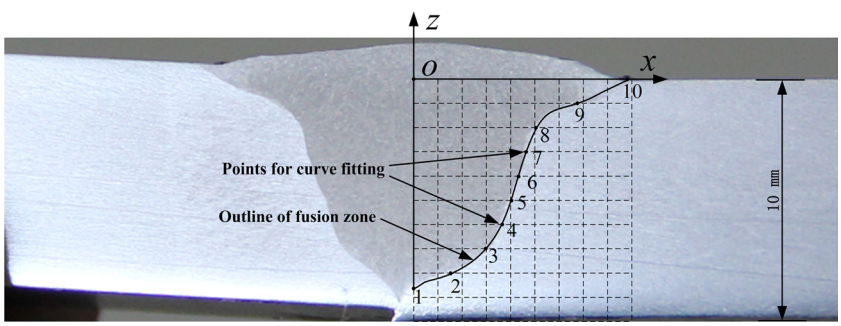

Fig. 1 Photograph showing the transverse cross section of a GMA butt weld and superimposed grid for 10-mm-thick HSLA plate

Table 1 Coordinates of points used to perform a polynomial curve fit of the fusion boundary for the GMA weld

Point	Coordinate Locations (z_i, x_i)
1	(−8.6, 0.0)
2	(−8.0, 1.5)
3	(−7.0, 3.0)
4	(−6.0, 3.7)
5	(−5.0, 4.0)
6	(−4.0, 4.3)
7	(−3.0, 4.6)
8	(−2.0, 5.0)
9	(−1.0, 6.7)
10	(0.0, 8. 8)

researchers have used separate plasma and weld pool models where the sheath regions are represented as simplified boundary conditions in order to achieve practical computational times [19, 20]. Some researchers have used constant temperature conditions to model the sheaths, but more recent studies have accounted for the large temperature gradient that exists across the sheath regions using a conductive model [21]. This approach was also used by Xu et al. [20] when simulating transport phenomena in GMA welding where the sheath regions were treated as special boundary conditions such that simplified source terms could be used to model heat transfer from the plasma to the anode and cathode. Applying this to a heat source model for arc welding, the use of a source term to simulate the sheath region is in effect equivalent to a separate heat source applied at the surface of the workpiece and also enables the arc to be decoupled.

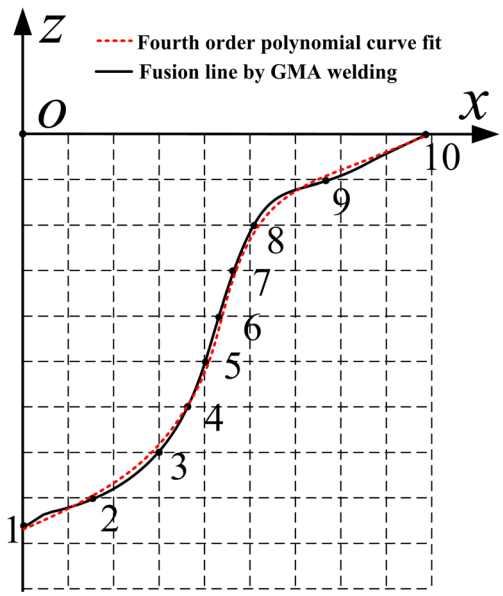

Fig. 2 Comparison of the actual fusion zone boundary and corresponding fourth order polynomial curve fit for a butt weld made on 10-mm-thick HSLA plate

While the heating radius on the surface will be a function of the arc diameter, this is difficult to establish in practice, and an effective heating radius must normally be inversed from the fusion zone cross section. For cross sections having a regular curvature, a suitable match can normally be achieved by optimizing the heat source parameters. However, for cross sections having an irregular curvature, a satisfactory representation may not be achieved due to limits of the function used in the heat source model. As such, the advantage of employing a separate disc source is that not only can it be used to adjust and refine the shape of fusion zone geometry and achieve an optimum fit with the actual weld cross section, but also it can also be used to account for other surface heating effects.

For a Gaussian surface heat source traveling at some velocity v, the heat flux distribution can be expressed in Cartesian coordinates as given in Eq. (3).

$$Q_s(x,y,t) = q_s \cdot \exp\left\{\frac{-3\left[x^2 + (y - vt)^2\right]}{r_o^2}\right\} \tag{3}$$

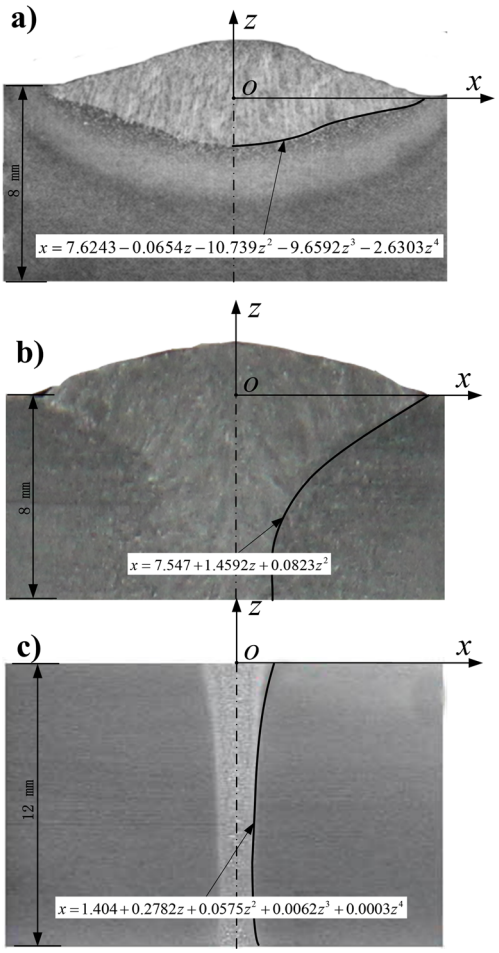

Fig. 3 Representative fusion zone boundaries with corresponding polynomial curve fit for **a** bead-on-plate, **b** GMA, and **c** laser welds

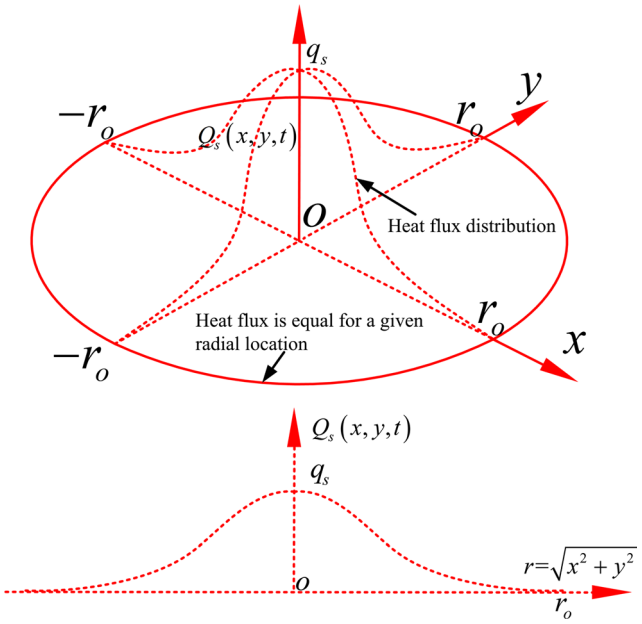

Fig. 4 Schematic representation of a Gaussian source and heat flux distribution

where $Q_s(x, y, t)$ is the heat flux at a point located on the top surface of the base metal at time t, q_s is the maximum heat flux, and r_o is the effective heating radius of the source.

As the fusion zone boundary is defined by a polynomial curve, the geometry of the volume heat source can be obtained by rotating the polynomial curve about the centerline of the weld. Assuming a Gaussian heat flux distribution, the resulting volume source component will be as shown in Fig. 5.

If the maximum weld penetration is taken to be h such that $(-h \le z \le 0)$, the heat density function of the volume heat source which is given by $Q_v(x, y, z, t)$ can then be expressed as shown in Eq. (4):

$$Q_v(x,y,z,t) = q_v \cdot \exp\left\{\frac{-3\left[x^2+(y-vt)^2\right]}{(a+bz+cz^2+dz^3+ez^4)^2}\right\} \quad (-h \le z \le 0) \tag{4}$$

where (x, y, z, t) represents a point which is located in or on the boundary of the fusion zone at time t, v is the welding speed, and q_v is the maximum heat flux. For the volumetric component used in the polynomial heat source model, the following assumptions were made. The maximum heat flux q_v is uniform along the source centerline through the weld thickness (along the z direction) and is considered to be collinear with the maximum heat flux q_s of the surface source.

A schematic showing the combined heat source is shown in Fig. 6, where the surface heat source component is depicted by the red contour line, while the black contour line represents the volume heat source component. While q_s and q_v are taken

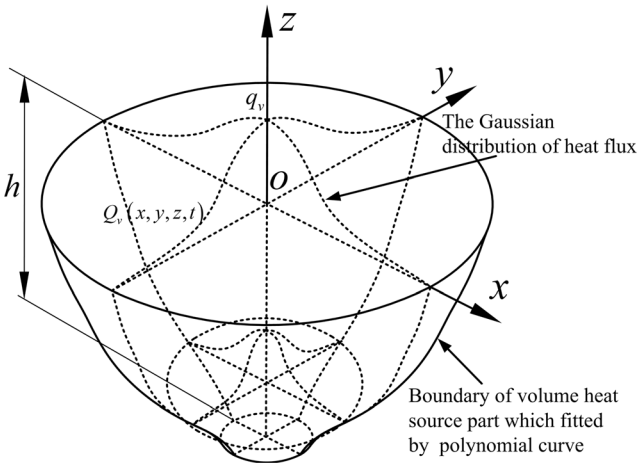

Fig. 5 Schematic representation of the volume heat model and Gaussian heat flux distribution for a weld of thickness h

as constant values, it should be noted that surface source is superposed on the volume source at the top surface of the plate. Consequently, the maximum power distribution will occur near the weld surface while the minimum will be at the weld root. Based on this approach, once a polynomial equation has been defined for the fusion zone, it is only necessary to determine suitable values for q_s, q_v, and r_o. As only three parameters need to be determined for the combined heat source model, this should also reduce the engineering effort that is needed to develop the necessary numerical values that must input a numerical model. As values for q_s, q_v, and r_o cannot be obtained directly from the weld cross section, it is necessary to use trial and error or a suitable inversion method until the simulated fusion outline from the FE model

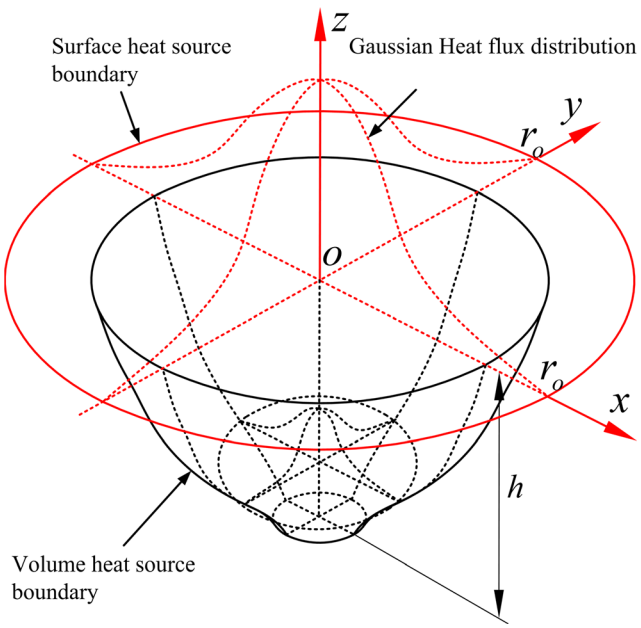

Fig. 6 Schematic of the combined heat source model represented in a Cartesian coordinate system

demonstrates satisfactory agreement with the actual fusion zone geometry.

3 Experimental setup

To validate the heat source model, GMA welding was used to butt weld high-strength low-alloy (HSLA) base metal pieces. ASTM A572-50 was selected as the base metal as it is a HSLA grade that has good weldability and is widely used to fabricate pressure vessels, piping, and on/off-shore structural members. The chemical composition of the ASTM A572-50 base metal is given in Table 2. All pieces were machined from hot-rolled plate in the as-received condition and had dimensions of 115 mm (length) × 62 mm (width) × 10 mm (thickness). A 30° bevel was also cut along one of the longitudinal edges such that a 60° single vee joint could be formed. A box-type resistance furnace was used to stress relieve all pieces before welding.

Prior to welding, two type K chromel-alumel thermocouples were mounted on the top surface of one of the pieces at the locations indicated as A and B in Fig. 7. The base metal pieces were then tack welded together at opposite ends of the vee joint. One piece was also tack welded to the support platform at the locations designated as M and N in Fig. 7 to act as a constraint. Both thermocouples were connected to a data acquisition system and personal computer so that the temperature history could be recorded during welding. Single pass butt welds were made using a CO_2 (20 %) + argon (80 %) shielding gas mix and 1.2-mm diameter wire electrode (ER-70S-3 AWS 5.28). A complete summary of the welding parameters that were used is given in Table 3.

As angular distortion and residual stresses represent additional metrics that can be used to indicate a heat source model's accuracy, these were also measured. Owing to the difficulty of directly measuring angular distortion along the weld line, dial indicators were mounted along the free edge at the locations designated C, D, and E in Fig. 7 and used to record the change in height after welding. As the differences between the three indicator readings were relatively small, the vertical deflection was obtained by taking an average of the three values.

Longitudinal and transverse residual stresses were measured after welding at six points located on the top surface. All points were taken at mid length and perpendicular to the travel direction as depicted by points 1–6 in Fig. 7. To ensure consistency, all stresses were measured using the same

Table 2 Chemical composition of the ASTM A572-50 base metal

Element	C	Mn	Si	S	P	Fe
wt%	0.23	1.35	0.3	0.05	0.04	Bal.

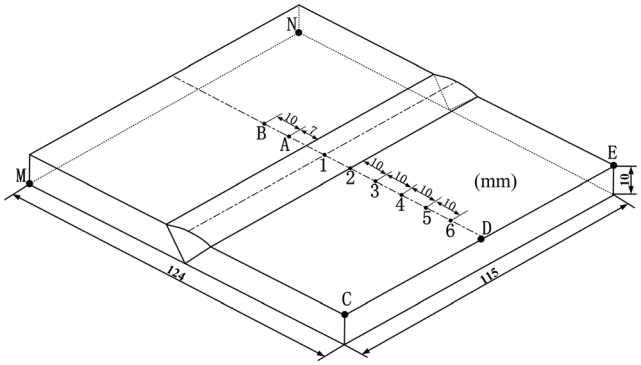

Fig. 7 Schematic of the welded plate indicating locations where experimental measurements were taken and constraints imposed

specimen. Electrolytic polishing was used to clean the surface of the weldment to ensure that additional stresses were not introduced. A Rigaku X-ray diffractometer was used to measure welding residual stresses using the fixed sin-squared-psi ($\sin^2 \Psi$) angle and side sloping method with three replications being taken at each point. Cross correlation was used to estimate the peak position. Crystal planes selected were (211) and angles were set at 0°, 25°, 35°, and 45°, respectively. The counting time was 0.50 s, the scanning step was set at 0.10°, and the scanning angle ranged from 151° to 163°.

4 FE simulation model

To simulate GMA welding, the commercially available SYSWELD FE software (ESI Corp.) was used. A fully coupled thermomechanical model was developed, and the element birth and death method was used to simulate formation of the weld bead. The weldment was modeled using 12250 8-node brick elements and the resulting FE mesh is shown in Fig. 8. Due to the steep thermal gradient that is generated during welding and the need to accurately map the outline of the predicted fusion zone, an element size of 1 mm × 1 mm × 3 mm was used in the region corresponding to the fusion and heat affected zones with 1 mm × 2 mm × 3 mm elements being used in the remainder of the plate to ensure conformity and to optimize the computation time. Displacement was fixed in all three directions at the

Table 3 Summary of experimental GMA welding conditions used

Condition	Values
Travel speed (mm/s)	3.7
Voltage (V)	25
Current (A)	275
Wire diameter (mm)	1.2
Heat input (J/mm)	1486.5
Shielding gas	CO_2 (20 %) + argon (80 %)

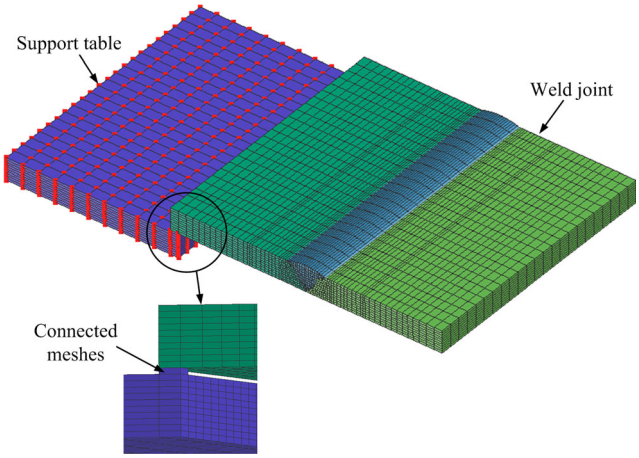

Fig. 8 FE mesh used in the GMA welding simulation model

locations designated as M and N in Fig. 7 to reflect the tack weld constraints that were used.

Thermal losses to the surrounding environment were modeled using element groups termed "skins" which consisted of 4-node quadrilateral elements superimposed on the free surfaces. As the plate was only supported at the bottom along the longitudinal edges, thermal conduction from the plate to each support was calculated according to Fourier's law which can be expressed as

$$\rho c\frac{\partial T}{\partial t}(x,y,z,t)-Q(x,y,z,t)=\nabla q(x,y,z,t) \tag{5}$$

where $Q(x,\ y,\ z,\ t)$ is a specified internal heat generation function per unit volume. This was calculated in SYSWELD by defining an appropriate mesh connection between the plate and the two supports.

Convective heat loss q_c was determined using Newton's law of cooling which is stated as

$$q_c=-h_f(T_{sfc}-T_{amb}) \tag{6}$$

where q_c is the convective heat loss, h_f is the convection coefficient and was specified to be equal to 15 W/m^2 °C, T_{sfc} is the surface temperature, and T_{amb} is the ambient temperature which was taken to be 20 °C.

Radiation losses from the plate q_r were calculated using the Stefan-Boltzmann law that is given as

$$q_r=-\varepsilon\sigma\left(T_{sfc}^4-T_{amb}^4\right) \tag{7}$$

where σ is the Stefan-Boltzmann constant, and ε is the emissivity which was specified to be equal to 0.8.

The base metal and weld material assumed to obey the von Mises yield criterion have isotropic properties and follow a kinematic hardening rule. Poisson's ratio and density were specified as 0.29 and 7966 kg/m^3, respectively, with both parameters considered to be independent of temperature. A melting temperature of 1430 °C was specified, and the remaining mechanical and physical parameters used to represent the ASTM A572-50 material were taken from the literature [22] and are shown as a function of temperature in Fig. 9. Due to the difficulty of obtaining mechanical and physical data over the full range of temperatures during welding, a linear extrapolation method was used to calculate values above 1200 °C.

5 Results and discussion

Prior to assessing the accuracy of the polynomial heat source model, it was of interest to analyze the effect that different mathematical functions had on the predicted fusion zone geometry. A GMA test weld was made using the conditions in Table 4 and a corresponding series of trial simulations were performed in SYSWELD using three different volumetric heat sources. These included the (a) fourth order polynomial, (b) double ellipsoid, and (c) conical heat sources. The primary objective was to determine how each function affected the shape of the predicted fusion zone for 10-mm-thick butt-welded steel plates having negligible crown of reinforcement. The simulation results are shown in Fig. 10, and it can be seen that in all three cases, the heat source predicted a semi-elliptical fusion zone cross section. While the dimensions of the predicted fusion zones do show some minor variation, the overall size and shape of the cross sections are consistent.

To test the effect that the order of the polynomial function had on the predicted fusion zone, a second series of trial simulations was performed using SYSWELD using the same weld, and the resulting fusion zone cross sections are shown in Fig. 11. First, second, and third order polynomials as well as a double ellipsoid heat source model were simulated. While no effect was made to analyze the effect of the coefficients, it can be seen that the order of the polynomial function does have some effect on the width and a minor influence on the overall shape. As each of the volumetric source components

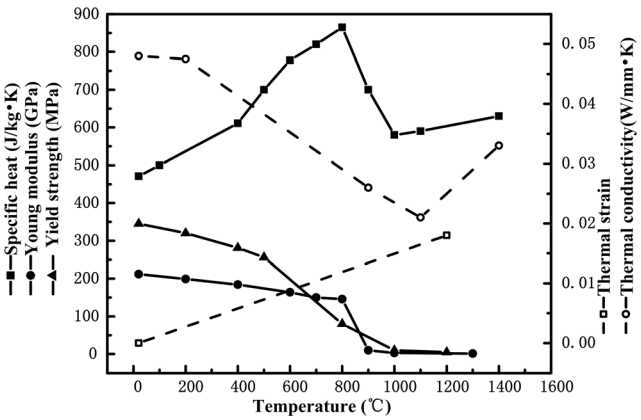

Fig. 9 Mechanical and thermophysical parameters of ASTM A572-50 steel shown as a function of temperature

Table 4 Summary of experimental conditions used to make the GMA test weld

Thickness (mm)	Current (A)	Voltage (V)	Travel speed (mm/s)	Heat input (J/mm)
10	140	16	0.8	2411.7

predicts a semi-elliptical cross section, this confirms that a second thermal component such as a disc source is useful to account for an "irregular curvature" and to adjust the shape of the fusion zone boundary.

5.1 Analysis of the predicted fusion zone

In order to further assess the polynomial heat source, double ellipsoid and conical heat source models were also used to simulate the experimental GMA welding conditions given in Table 3. Coefficients for the double ellipsoid and conical heat sources were obtained using the inversion procedure proposed by Chen et al. [10], and the resulting equations and coefficients for all three heat source models are summarized in Table 5. A desktop personal computer equipped with a single core Intel processor was used to perform all FE simulations. The CPU time using the polynomial heat source was 19 min, while the corresponding simulation times for both the double ellipsoid and conical heat source models were 20 min. This result confirms that all three heat sources have comparable computational costs.

Digitized images of the experimental and predicted fusion zone outlines from all three heat source models were analyzed and are shown in Fig. 12. Based on the simulated and experimental fusion zone outlines shown in Fig. 12, it is evident that the polynomial heat source model demonstrates the best overall agreement with only 8.7 % difference in cross-sectional area. The difference between the predicted and actual cross-sectional area for the double ellipsoid and 3D conical sources was 24.2 and 27.2 %, respectively. In comparison, the size and shape of the fusion zone predicted by the double ellipsoid and 3D conical Gaussian heat source models can be seen to be quite similar to each other though both tend to underpredict the fusion zone width near the top of the

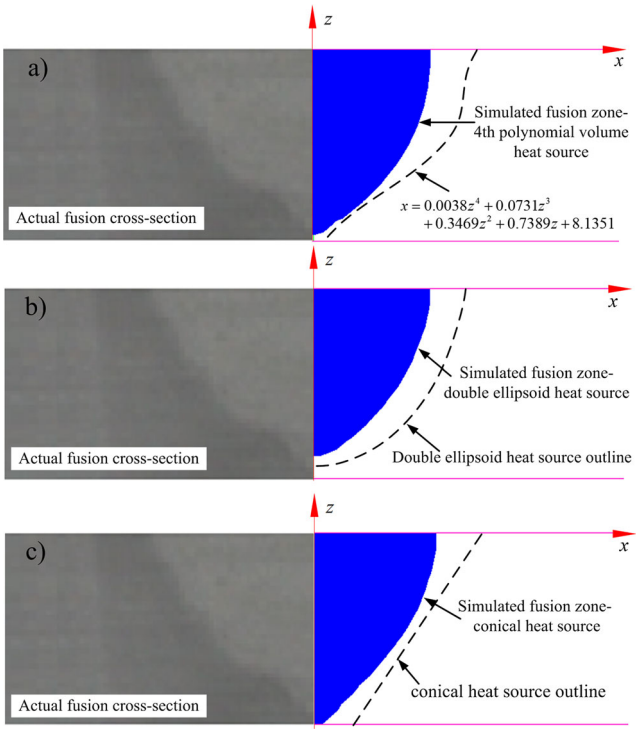

Fig. 10 Comparison of predicted fusion zone obtained from SYSWELD FE simulations using **a** polynomial, **b** double ellipsoid, and **c** conical heat source models with actual GMA weld in 10-mm-thick HSLA plate

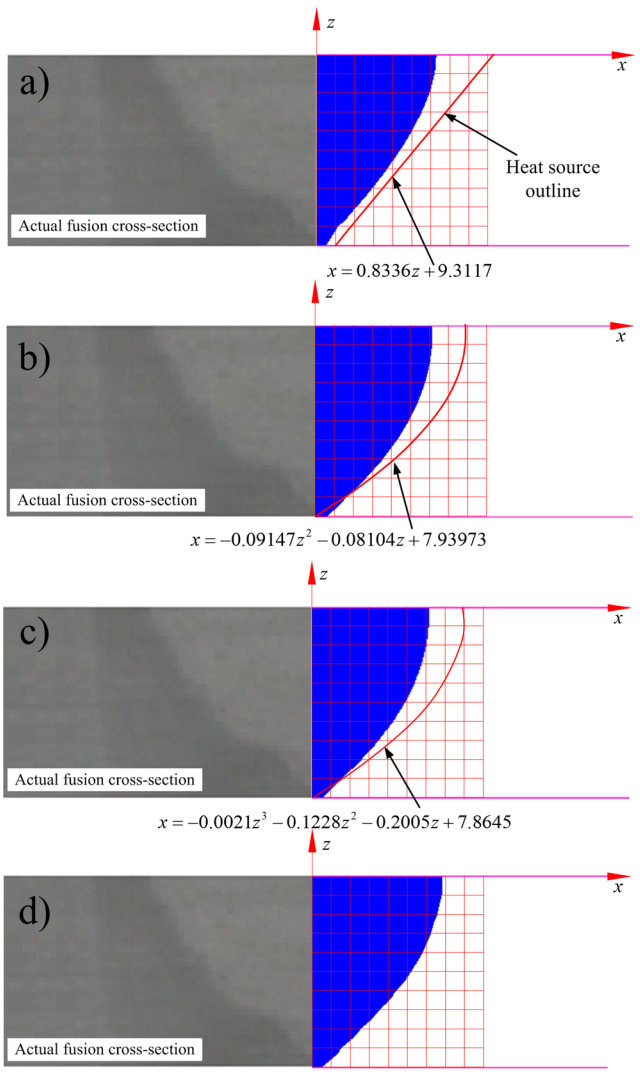

Fig. 11 Comparison of predicted fusion zone outlines using **a** first, **b** second, and **c** third order polynomials and d) double ellipsoid volume heat source models

Table 5 Summary of equations and coefficients for the heat source models used in the SYSWELD simulation model

Heat source model	Mathematical representation	Coefficient values
Double ellipsoid	$\begin{cases} q_f(x,y,z,t) = \frac{\sqrt[6]{3q_f}}{a_f bc\pi\sqrt{\pi}} \exp\left(-\frac{3x^2}{a_f{}^2} - \frac{3(y-vt)^2}{b^2} - \frac{3z^2}{c^2}\right), & y \geq 0 \\ q_r(x,y,z,t) \frac{\sqrt[6]{3q_r}}{a_r bc\pi\sqrt{\pi}} \exp\left(-\frac{3x^2}{a_r{}^2} - \frac{3(y-vt)^2}{b^2} - \frac{3z^2}{c^2}\right), & y < 0 \end{cases}$	$q_f = 8, q_r = 5, a_f = 5,$ $a_r = 10, b = 8, c = 7.2$
Conical	$q(x,y,z,t) = q_o \cdot \exp\left\{\frac{-3\left[x^2+(y-vt)^2\right]}{\left(\frac{(z-z_e)(r_e-r_i)}{z_e-z_i} r_e\right)^2}\right\}$	$q_o = 11, r_e = 11, , r_i = 1,$ $z_e = 5, z_i = -10$
Polynomial	$\begin{cases} Q_s(x,y,t) = q_s \cdot \exp\left\{\frac{-3\left[x^2+(y-vt)^2\right]}{r_o{}^2}\right\} \\ Q_s(x,y,z,t) = q_s \cdot \exp\left\{\frac{-3\left[x^2+(y-vt)^2\right]}{(a+bz+cz^2+dz^3+ez^4)^2}\right\} (-h \leq z \leq 0) \end{cases}$	$q_s = 3.2,\ q_v = 10,\ r_o = 20$

plate and overpredict it in the remainder of the cross section. This is attributable to the lack of capability in these two sources to independently control/optimize the power distribution at the top and bottom of the weld in order to match the nailhead cross section.

While some small differences in width and curvature can be seen in the regions above the root and below the toe, based on the results shown in Fig. 13, it is evident that the predicted fusion zone from the polynomial heat source model demonstrates overall good agreement with the actual weld geometry and reasonably reflects the irregular curvature. The most likely cause for slightly overestimating the width in the top half of the bead is that the flux on the trailing side of the arc is likely less intense and has some deviation from the symmetric radial distribution used in the model.

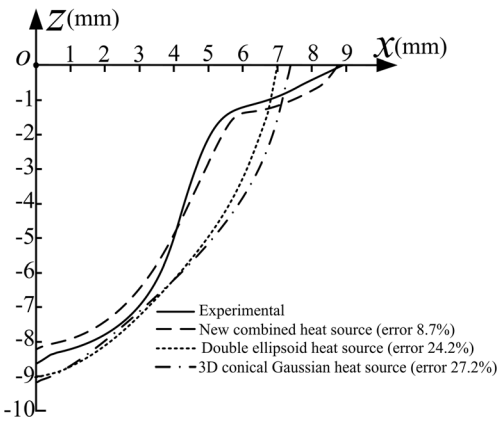

Fig. 12 Comparison of predicted fusion lines obtained using different heat source models and actual bead geometry for butt welds made on 10-mm-thick HSLA plate

5.2 Analysis of thermal cycles during GMA welding

The simulated thermal cycles obtained from each heat source are shown in Fig. 14 along with the experimental curves that were collected during welding. It can be seen that the maximum temperature of 567.3 °C occurred 37.2 s after the start of welding at the location adjacent to the weld toe (point A). Similarly, at the second location (point B), the peak temperature of 362.7 °C occurred at 60.7 s. Upon examination of Fig. 14, it can be seen that the thermal cycles from each of the heat source models show similar trends and that the peak temperatures predicted at both locations are quite close and vary by less than 5 °C. While all three models demonstrate essentially identical behavior during heat-up, some differences are evident during cooling. At the onset of cooling, the double ellipsoid and conical heat sources tend to overestimate cooling rate and predict a more rapid drop-off in temperature at both locations until an equilibrium temperature of 225 °C is achieved in the plate at 350 s. In comparison, it can be seen that the thermal cycle curves from the polynomial heat source more closely follow and provide the best agreement with the experimental curves at both locations during cooling though temperature is slightly overestimated by about 2 °C after 150 s. The most likely reason for the difference in cooling behavior is due to the larger effective heating radius of the disc source used in the polynomial model that tended to supply more heat to the trailing side nodes after the heat source had passed.

5.3 Comparison of angular distortion

The average vertical deflection resulting from GMA welding and the simulated values obtained from each of the heat

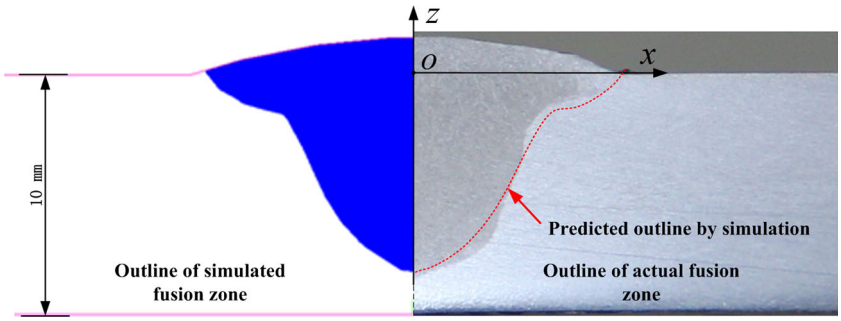

Fig. 13 Comparison of the predicted fusion zone obtained using the combined polynomial heat source and experimental GMA welding for 10-mm-thick HSLA plate

sources are given in Table 6. Based on the values shown in Table 6, it can be seen that the percent error from the polynomial, double ellipsoid, and conical heat sources was −8.3, −21, and −24.2 %, respectively. While all three sources tended to underestimate the deflection, it can be seen that the polynomial heat source provided a more accurate prediction of the angular distortion.

The most likely reason for the differences in predicted deflection is due to the geometry of the plastic strain zone which is the source of a bending moment and resulting angular distortion as noted by Yang et al. [23]. To assess this, the transverse plastic strain zones predicted by each of the heat source models are shown in Fig. 15. In order to better delineate the outline of the plastic zone, only the elastic contour values are shown. It can be seen that the plastic strain zone for the double ellipsoid and 3D conical Gaussian sources is quite similar in size and shape, whereas that of the polynomial heat source shows more variation and has a more pronounced trough and curvature which would indicate a higher bending moment and resulting vertical deflection.

5.4 Comparison of residual stresses

Longitudinal and transverse residual stress values corresponding to the six surface locations on the weldment are shown in Fig. 16. The experimental data in Fig. 16 show that the maximum longitudinal and transverse stress values were found to be 148 and 178 MPa, respectively, and that both occurred at the weld toe. While the predicted stresses from all three heat sources show some deviation from the measured values, the overall trends demonstrate good agreement with the experimental curves. However, it is evident from both cases in Fig. 16 that the polynomial heat source tends to predict higher tensile values in the vicinity of the fusion zone and gives slightly better overall agreement with experimental stresses.

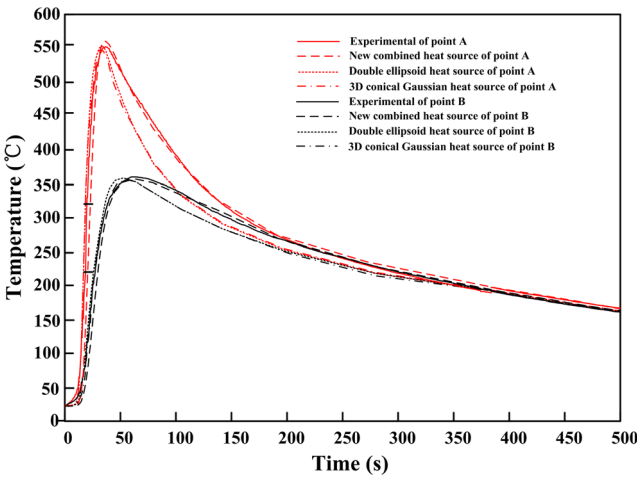

Fig. 14 Comparison of predicted and actual thermal cycles during GMA welding of the HSLA plate

6 Summary and conclusions

In the present study, a combined surface and volumetric heat source model was proposed for simulating single pass welds with symmetric fusion zones. The proposed model is based on a polynomial function that is used to represent the volumetric source and a disc source which is superimposed on the surface. Future work will focus on extending the heat source model to simulate an asymmetric weld cross section as well as analyzing fillet welds where the symmetry requirement is met. Based on the results that were obtained, the following conclusions can be made:

1. The fusion boundary of most welds can be represented using a polynomial function of four orders or less.
2. The fusion zone geometry predicted by the polynomial heat source model demonstrated the best agreement with the experimental weld cross section. Analysis of the weld cross section showed that the corresponding percent difference in area was 8.7 %. In comparison, the percent

Table 6 Summary of average vertical distortions and percent error obtained using different heat source models

Heat source	Average distortion (mm)	Percent error
Actual	1.57	\
Polynomial	1.44	−8.3
Double ellipsoid	1.24	−21.0
Conical	1.19	−24.2

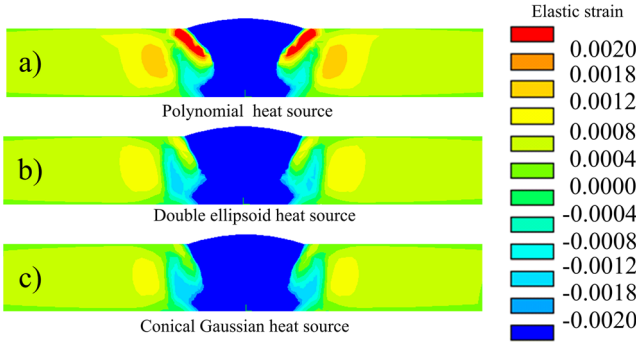

Fig. 15 **a**–**c** Comparison of transverse plastic strain zone geometries predicted by each of the heat source models

difference in area from the double ellipsoid and conical heat source models was 24.2 and 27.2 %, respectively.

3. Initial heat-up and peak temperatures from all three heat source models were comparable and show good agreement with thermocouple measurements taken from the plate surface. During cooling, the polynomial model provided better agreement than the double ellipsoid and conical sources which tended to have more rapid cooling rates until thermal equilibrium was achieved in the plate.
4. The angular distortion was underestimated by all three heat source models. However, when compared to experimental measurements, the predictions from the polynomial heat source model showed the best agreement with less than 10 % error from the actual plate deflection.
5. There was good overall agreement between the simulated and actual residual stress profiles for all three heat source models. The difference in predicted longitudinal and transverse residual stress values was negligible outside of the fusion zone though the polynomial heat source model showed slightly better agreement for longitudinal and transverse tensile stresses measured in the vicinity of the weld bead.

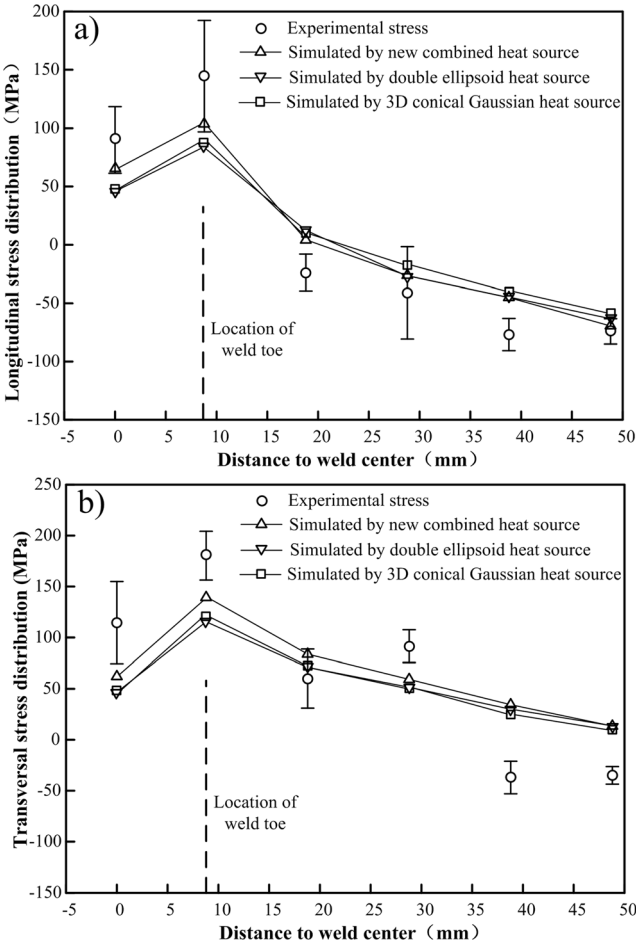

Fig. 16 Comparison of simulated residual stresses obtained using selected heat source models and experimental measurements showing **a** longitudinal and **b** transverse stress distributions in the welded HSLA plate

Acknowledgments The authors would like to acknowledge the support of the National Natural Science Foundation of China (Grant No. 51271014).

References

1. Chen Y, He Y, Chen H, Zhang H, Chen S (2014) Effect of weave frequency and amplitude on temperature field in weaving welding process. Int J Adv Manuf Technol 75(5–8):803–813
2. Pavelic V, Tanbakuchi R, Uyehara O, Myers P (1969) Experimental and computed temperature histories in gas tungsten-arc welding of thin plates. Weld J 48(7):295s–305s
3. Rosenthal D (1946) The theory of moving sources of heat and its application to metal treatments. Trans Am Soc Mech Eng 43(11): 849–866
4. Wenji L, Liangyu L, Jianfeng Y, Haihua L, Lei Y (2015) A kind of analytical model of arc welding temperature distribution under varying material properties. Int J Adv Manuf Technol 81(5): 1109–1116
5. Goldak J, Chakravarti A, Bibby M (1984) A new finite element model for welding heat sources. Metall Mater Trans B 15(2):299–305
6. Paley Z, Hibbert P (1975) Computation of temperatures in actual weld designs. Weld J 54(11):385s–392s
7. Wu S, Zhao H, Wang Y, Zhang X (2004) A new heat source model in numerical simulation of high energy beam welding. Trans Chin Weld Inst 25(1):91–94
8. Li X, Wang L, Yang L, Wang J, Li K (2014) Modeling of temperature field and pool formation during linear laser welding of DP1000 steel. J Mater Process Technol 214(9):1844–1851
9. Bachorski A, Painter M, Smailes A, Wahab M (1999) Finite-element prediction of distortion during gas metal arc welding using the shrinkage volume approach. J Mater Process Technol 92:405–409
10. Chen Y, Han J, Li Z, Xia L, Yang Z (2014) An inverse method for searching parameters of combined welding heat source model. Inverse Prob Sci Eng 22(6):1009–1028
11. Faraji A, Goodarzi M, Seyedein S, Barbieri G, Maletta C (2015) Numerical modeling of heat transfer and fluid flow in hybrid laser–TIG welding of aluminum alloy AA6082. Int J Adv Manuf Technol 77(9–12):2067–2082
12. Meng X, Qin G, Su Y, Fu B, Ji Y (2015) Numerical simulation of large spot laser + MIG arc brazing–fusion welding of Al alloy to galvanized steel. J Mater Process Technol 222:307–314

13. Chukkan J, Vasudevan M, Muthukumaran S, Kumar R, Chandrasekhar N (2015) Simulation of laser butt welding of AISI 316L stainless steel sheet using various heat sources and experimental validation. J Mater Process Technol 219:48–59
14. Murphy A, Tanaka M, Yamamoto K, Tashiro S, Lowke J, Ostrikov K (2010) Modelling of arc welding: the importance of including the arc plasma in the computational domain. Vacuum 85(5):579–584
15. Carmignani C, Mares R, Toselli G (1999) Transient finite element analysis of deep penetration laser welding process in a singlepass butt-welded thick steel plate. Comput Methods Appl Mech Eng 179(3):197–214
16. Zhang L, Gao X, Sun M, Zhang J (2014) Weld outline comparison between various pulsed Nd: YAG laser welding and pulsed Nd: YAG laser–TIG arc welding. Int J Adv Manuf Technol 75(1–4): 153–160
17. Li S, Chen G, Zhou C (2015) Effects of welding parameters on weld geometry during high-power laser welding of thick plate. Int J Adv Manuf Technol 79(1–4):177–182
18. Luo Y, You G, Ye H, Liu J (2010) Simulation on welding thermal effect of AZ61 magnesium alloy based on three-dimensional modeling of vacuum electron beam welding heat source. Vacuum 84(7):890–895
19. Wu C, Gao J (2002) Analysis of the heat flux distribution at the anode of a TIG welding arc. Comput Mater Sci 24(3):323–327
20. Xu G, Hu J, Tsai H (2009) Three-dimensional modeling of arc plasma and metal transfer in gas metal arc welding. Int J Heat Mass Transf 52(7):1709–1724
21. Li Y, Feng Y, Li Y, Zhang X, Wu C (2016) Plasma arc and weld pool coupled modeling of transport phenomena in keyhole welding. Int J Heat Mass Transf 92:628–638
22. Wang J, Han J, Domblesky J, Li W, Yang Z, Zhao Y (2015) Predicting distortion in butt welded plates using an equivalent plane stress representation based on inherent shrinkage volume. J Manuf Sci Eng 138(1):011012–011012
23. Yang Y, Athreya B (2013) An improved plasticity-based distortion analysis method for large welded structures. J Mater Eng Perform 22(5):1233–1241